Bundles Consisting of Extended Transmembrane Segments of Vpu from HIV-1: Computer Simulations and Conductance Measurements†

F. S. Cordes,‡ A. D. Tustian,§ M. S. P. Sansom,‡ A. Watts,§ and W. B. Fischer*,§

Biomembrane Structure Unit and Laboratory of Molecular Biophysics, Department of Biochemistry, Oxford University, South Parks Road, Oxford OX1 3QU, U.K.

Received January 7, 2002; Revised Manuscript Received March 20, 2002

ABSTRACT: Part of the genome of the human immunodeficiency virus type 1 (HIV-1) encodes for a short membrane protein Vpu, which has a length of 81 amino acids. It has two functional roles: (i) to downregulate CD4 and (ii) to support particle release. These roles are attributed to two distinct domains of the peptide, the cytoplasmic and transmembrane (TM) domains, respectively. It has been suggested that the enhanced particle release function is linked to the ion channel activity of Vpu, with a slight preference for cations over anions. To allow ion flux across the membrane Vpu would be required to assemble in homooligomers to form functional water-filled pores. In this study molecular dynamics simulations are used to address the role of particular amino acids in 4, 5, and 6 TM helix bundle structures. The helices (Vpu_{6-33}) are extended to include hydrophilic residues such as Glu, Tyr, and Arg (EYR motif). Our simulations indicate that this motif destabilizes the bundles at their C-terminal ends. The arginines point into the pore to form a positive charged ring that could act as a putative selectivity filter. The helices of the bundles adopt slightly higher average tilt angles with decreasing number of helices. We also suggest that the helices are kinked. Conductance measurements on a peptide (Vpu_{1-32}) reconstituted into lipid membranes show that the peptide forms ion channels with several conductance levels.

The genome of the human immunodeficiency virus type 1 (HIV-1)[1] encodes a short auxiliary membrane protein, 81 amino acids in length, called Vpu (*1*, *2*). Its biological role in the life cycle of HIV-1 is to downregulate the presence of CD4 protein in the cell membrane of the infected cell via its cytoplasmic C-terminal tail (*3*−*6*) and to support the release of virus particles via its transmembrane (TM) N-terminal segment (*7*−*9*). Recently, it has been found that Vpu also downregulates the major histocompatibility complex 1 (MHC 1) in the infected cell (*10*).

Ion channel activity, with a slight preference for cations, has been demonstrated for Vpu transcribed in *Xenopus* oocyte cells measuring whole cell currents under voltage clamp conditions (*7*). Vpu expressed in *Escherichia coli* and reconstituted into lipid bilayers also exhibits channel activity (*11*). Studies with constructs representing the TM segment of Vpu reconstituted into bilayers confirm that its channel activity is connected with the N-terminal end of the protein (*7*). Findings that Vpu forms homooligomers in the presence of lipid membranes provide evidence that channel activity is most likely a result of the formation of parallel, aligned homooligomers (*12*). The exact number of segments forming the channels is yet to be evaluated with biophysical methods. However, despite this evidence, there are also studies which question channel activity of Vpu (*13*), assigning the role of Vpu to destabilize host cell membrane proteins. A proof of channel activity for Vpu would be the discovery of selective channel blockers (*14*). Recently, such blockers have been described: channel activity of Vpu, and its peptide analogous to the TM domain reconstituted in black lipid membranes, can be blocked by derivatives of amiloride (*15*). In vivo analysis also revealed a reduced number of virions being released from the infected cell in the presence of the amiloride derivatives.

CD and solution-state NMR spectroscopy have been used to elucidate the structure of the cytoplasmic domain of Vpu (*16*−*18*). All NMR spectroscopic investigations have in common a helix−interconnection−helix motif while any further motif toward the C-terminus beyond this one depends on the applied experimental condition. Structural data for the TM domain of Vpu have been derived from solid-state NMR spectroscopy. Studies with the TM domain reconstituted into lipid bilayers indicate that the segment is tilted at less than 30° with respect to the membrane normal (*19*). With uniformly ^{15}N-labeled full-length Vpu, a tilt angle of ca. 15° is found (*20*). FTIR dichroism spectroscopy with a synthetic construct representing the TM segment of Vpu suggests an tilt angle of ca. 6.5° (*21*).

† W.B.F. thanks the EC for a TMR research fellowship. F.S.C. was supported by the Deutsche Volk Stiftung. A.W. thanks the BBSRC for a BBSRC Research Fellowship grant.

* Corresponding author. E-mail: wolfgang.fischer@bioch.ox.ac.uk. Tel: +44-1865-275776. Fax: +44-1865-275234.

‡ Biomembrane Structure Unit.

§ Laboratory of Molecular Biophysics.

[1] Abbreviations: HEPES, *N*-(2-hydroxyethyl)piperazine-*N*′-2-ethanesulfonic acid; HIV-1, human immunodeficiency virus type 1; MHC 1, major histocompatibility complex 1; NMR, nuclear magnetic resonance; POPC, 1-palmitoyl-2-oleoyl-*sn*-glycero-3-phosphatidylcholine; POPE, 1-palmitoyl-2-oleoyl-*sn*-glycero-3-phosphoethanolamine; RMSD, root mean square deviation; SA/MD, simulated annealing and restrained molecular dynamics; SEM, standard error of mean; TFE, tetrafluoroethanol; TM, transmembrane.

10.1021/bi025518p CCC: $22.00
Published on Web 05/15/2002

Two computational approaches have been used to model bundles of helices forming a water-filled pore. In one approach, bundles consisting of 4, 5, and 6 helices were placed in a slab representing a lipid bilayer with low dielectric (*22*). Serines were oriented toward the interior of the bundle. The helices were restrained during the simulation. Also, the water molecules were held within the mouth of the bundle during the simulation. The simulations confirmed the slight cation preference found experimentally and suggested a homopentamer to be the overall motif for Vpu. In another study, two hydrated pentameric bundles with the same sequence were embedded in octane, a bilayer mimetic (*23*). Simulations have been performed without any restraints on the peptide helices. One of the models was built according to the models in ref *22* with the serines facing the pore. A second model was built by placing all of the tryptophans so that they face the pore. Both structural models include the disappearance of a continuous water column within the bundle as a common feature. The data are interpreted in terms of a non-ion-conducting pore. An average tilt angle of the helices with respect to the octane slab normal was calculated to be 4.2°. For the model where the tryptophan's orientation was imposed, a more detailed simulation has been undertaken with pentameric bundles in a fully hydrated lipid bilayer (*24*). All models retain a water-filled pore, and the tryptophans remain in the pore after the simulations (2 ns).

In this study we have extended the computer simulations by using an extended model of Vpu with 28 amino acids, Vpu_{6-33}, embedded in an explicit lipid bilayer environment: Vpu_{6-33}, IVAIV[10] ALVVAIIIAI[20] VVWSIVIIEY[30] RKI. With this model we are able to focus not only on the residues within the TM region but also on particular residues such as glutamic acid, tyrosine, and arginine (EYR motif), which are suggested to be involved in the bend between the TM helix and the first extramembraneous helix (*25*). This helix lies with its helix long axis parallel to the membrane surface (*20*).

MATERIALS AND METHODS

We generated bundles consisting of 4 (bundle 4), 5 (bundle 5), and 6 (bundle 6) helices using a simulated annealing and restrained molecular dynamics (SA/MD) protocol (*26*) based on the program X-PLOR (*27*). A starting tilt angle of 5° was implemented during the generation process. A detailed description of the generation of the TM helices is given elsewhere (*24*, *26*). In brief, the SA/MD protocol comprises two stages: In stage 1 the bundles are constructed with parallel, idealized α-helices based on the positions of the Cα atoms of the peptide unit. All other atoms of the individual amino acids are superimposed. During stage 1 a repulsive van der Waals term is slowly introduced after an initial delay to allow the individual atoms to pass each other. We obtained five structures for each bundle. Each structure from stage 1 is used for five molecular dynamics runs in stage 2. In stage 2 potential energy functions with the PARAM19 parameter set are introduced in the protocol. Partial charges on side-chain atoms of polar side chains are gradually scaled up (from 0.05 to 0.4 times their full value) during a temperature reduction from 500 to 300 K. The scaling factor 0.4 is also applied during the 5 ps dynamics and energy minimization. Harmonic restraints hold the Cα atoms but are relaxed as the temperature is dropped from 500 to 300 K. At this stage distance restraints are also introduced. In stage 2 we obtained $5 \times 5 = 25$ structures. The most symmetric structure with respect to the pseudo-5-fold symmetry axis of the bundle was chosen for the simulations.

Bundles consiting of 4, 5, and 6 helices derived from the X-PLOR protocol as outlined above were placed within a lipid bilayer of 1-palmitoyl-2-oleoyl-*sn*-glycero-3-phosphatidylcholine (POPC) and consequently solvated with more than 30 water molecules [SPC water model (*28*)] per lipid, resulting in a system of ca. 20000 atoms (*29*) (Figure 1A). Two minimizations were run as part of the construction of the hydrated bundle/bilayer system and a short equilibration run of 100 ps. Simulations were run for 1 ns using GROMACS 1.6 software (http://rugmd0.chem.rug.nl/~gmx/gmx.html) on a 10 processor SGI Origin 2000 machine. Gromacs software was used for data analysis. The structures were visualized with the program MOLSCRIPT.

Channel Recordings in Planar Lipid Bilayers. The peptide corresponding to the N-terminal side of Vpu, MQPIPIVAIV[10] ALVVAIIIAI[20] VVWSIVIIEY[30] RK (MW 3544), was obtained from G. Ewart and P. Grage, Australia National University. A detailed description of the peptide synthesis and purification is given elsewhere (*15*). An Applied Biosystems Model 477a machine was used for the synthesis followed by purification with a reversed-phase HPLC using a RP304 column (Bio-Rad).

A planar lipid bilayer was formed across an elliptical aperture (ca. 120 μm diameter on the long axis) in a thin (25 μm) Teflon film (Yellow Springs Instruments, Yellow Springs, OH) (*30*). Lipids [ca. 40 μL of a 4:1 (w/w) mixture of 1-palmitoyl-2-oleoyl-*sn*-glycero-3-phosphoethanolamine (POPE) and 1-palmitoyl-2-oleoyl-*sn*-glycero-3-phosphocholine (POPC) dissolved in pentane to 5 mg/mL] were spread on top of an aqueous subphase (0.5 M KCl, 5 mM HEPES, 1 mM $CaCl_2$, pH 7.4). This resulted in ca. 0.2 mg of lipid on each side of the aperture. Evaporation of the pentane solvent took place over a 10 min incubation period. The bilayer was then formed by raising the buffer level over the hole in the Teflon film. After formation of a stable bilayer the peptide [dissolved in tetrafluoroethanol (TFE)] was added from a 200-fold excess stock solution to the aqueous subphase of the trans side (electrically grounded) to reach a final concentration of ca. 30 μM (each of the chambers on either side of the bilayer had a volume of 2 mL of liquid inside). Recordings appeared after a time delay of ca. 35 min. Electrical currents were recorded with an Axopatch 1D amplifier at a rate of 5 kHz and filtered with 1 kHz using a Digi Data 1200 interface (Axon Instruments). Currents were generated using a Function Generator TG 302, LEVELL, Barnet, U.K.

RESULTS

The putative TM region of Vpu includes a single hydrophilic residue, serine. We constructed all bundles in this study with the assumption that hydrophilic residues such as serines are lining the ion-conducting pore of a putative channel. This assumption is based on molecular modeling studies on other ion channels (*31*−*33*). The root mean square deviation (RMSD) for all bundles levels off after ca. 100 ps and does not exceed a value of 0.3 nm (Figure 1B). This is in

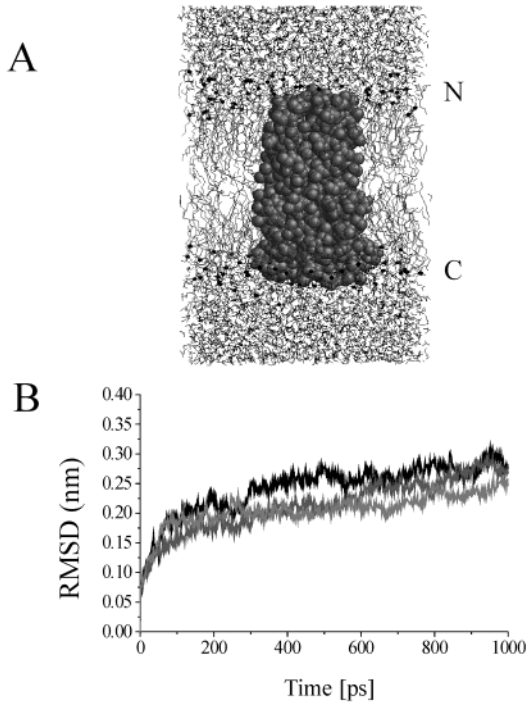

FIGURE 1: (A) A fully hydrated pentameric bundle/bilayer system as used in the simulations. Gray: helical segments of the TM segment of Vpu (5 × 28 amino acids = 1345 atoms). Light gray: lipid bilayer with small black balls defining the phosphorus atoms of the lipid headgroups (96 lipids = 4992 atoms). Dark gray: small angles above and below the bilayer represent solvent molecules (4254 water molecules = 12762 atoms). The simulation box consists of a total of 19119 atoms. (B) RMSD of Cα atoms versus time calculated from the starting structure: black, bundle 4; gray, bundle 5; light gray, bundle 6.

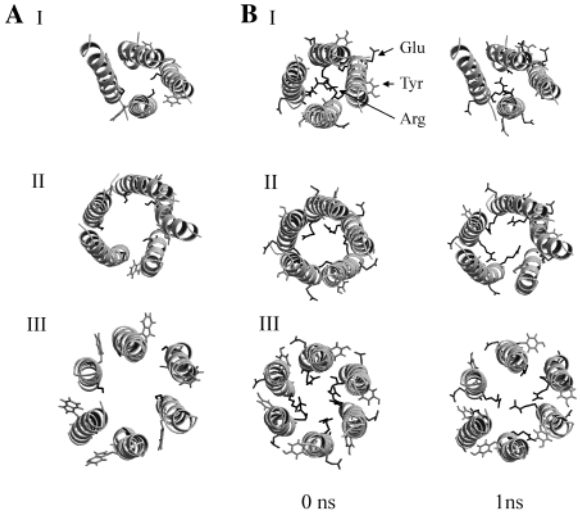

FIGURE 2: (A) View from the N-terminal end to the C-terminal end for the tetramer (I, bundle 4), pentamer (II, bundle 5), and hexamer (III, bundle 6) of Vpu after 1 ns of simulation. Serine side chains are shown in black and tryptophans in gray. The lipid bilayer and water molecules are omitted for clarity. (B) Same view for the oligomers as in (A) at 0 ns (left panel) and 1 ns (right panel). Black residues denote arginines, light gray residues tyrosines, and gray residues glutamic acids.

accordance with other successfully conducted simulations on other TM bundles (*33*, *34*).

Figure 2 shows the structure of the bundles with a view down the pore from the N- to the C-terminus. After the 1 ns simulations all residues highlighted (Figure 2) retain their pore-facing position. In bundle 4 it seems that one helix tilts away from the bundle with its N-terminal end during a 1 ns simulation (Figure 2A, I, left segment in the bundle on the right). Another helix of bundle 4 adopts a large kink angle of ca. 32° (Table 1 and I in Figure 2A). The side chains of glutamic acids (gray), tyrosines (light gray), and arginines (black) within the bundles at the beginning and at the end of the simulations are shown in Figure 2B. At the beginning of the simulations, all arginines are pointing into the interior of the bundles. During the simulation repulsive forces move at least two arginines out of the pore in bundle 4 and bundle 6.

Table 1: Structural Data and Conductivity of Bundles 4, 5, and 6[a]

	Vpu-4	Vpu-5	Vpu-6
structural data			
kink angle (deg)	16.9 ± 10.0 32.1 ± 1.9	19.9 ± 7.8	12.7 ± 7.7
tilt angle (deg)	15.3 ± 5.0	14.5 ± 3.4	6.0 ± 2.1
crossing angle (deg)	20.2 ± 7.5	16.7 ± 2.2	4.6 ± 2.3
conductivity (pS)			
0.5 M KCl	12.2 ± 4.1	52.2 ± 5.0	51.9 ± 2.5
0.5 M NaCl	6.7 ± 2.5	32.0 ± 3.0	21.4 ± 2.8
no. of waters	3	92	108
min pore radius (Å)	0.7	2.5	2.3
exptl, 0.5 M KCl	20.7 ± 2.3 (3) ~30*	59.3 ± 4.2 (5) ~107*	137.0 ± 5.4 (5)

[a] Structural data reflect an average over the data *n* ranging from 500 to 1000 ps in steps of 50 ps (11 values) and over the values for each segment ($n \times 11$ values in total, with $n = 4$, 5, and 6 for bundles 4, 5, and 6, respectively). The standard deviation of these values is given. The number of water molecules is estimated from visible inspection of the models. The experimental conductance values are given as mean ± SEM. Numbers in parentheses indicate the number of means accounting for the values. Asterisked values derive from single events found in the traces.

From the N-terminal end to Ile-28 all helices in all of the bundles remain in a helical conformation with ϕ- and ψ-values around −60° and −50° (*35*), respectively. In one helix of bundle 4, Ser-24 deviates from normality with an average ϕ of (−28.6 ± 20.4)° [corresponding ψ = (−52.0 ± 12.2)°] and causes the strong bend (see Figure 2A, I). The ϕ and ψ values for the EYR motif are listed in Table 2. The values of the Glu-29, Tyr-30, Arg-31, and Lys-32 of those helices are shown if they deviate more than half the value for an ideal helix. For bundle 4 two helices are listed in which Arg-31 [ϕ = (−140.2 ± 20.5)° and ψ = (94.4 ± 13.5)° in first helix; ϕ = (−69.4 ± 18.2)° and ψ = (−10.5 ± 27.3)° in second helix] and Lys-32 [ϕ = (−117.7 ± 15.9)° and ψ = (−73.8 ± 18.0)° in first helix] show the most pronounced deviation. For bundle 5 two helices could be identified in which Tyr-30 [ϕ = (−63.8 ± 10.9)° and ψ = (−23.1 ± 16.2)° in one helix; ϕ = (−30.1 ± 13.8)° and ψ = (−49.7 ± 11.6)° in second helix] and Lys-32 [ϕ = (−53.6 ± 13.4)° and ψ = (−24.2 ± 14.2)° in one helix] adopt values just around the defined limits (Table 2). In bundle 6 strong deviations are found for the Glu-29, Tyr-30, Arg-31, and the Lys-32 in one helix. In an additional helix only Arg-31 and Lys-32 show large deviations. These results indicate that in bundles with more helices those helices remain in a more helical conformation at the C-terminal end.

The average values over all helices within a bundle for the kink, tilt, and crossing angles are shown in Figure 3. A

Table 2: ϕ- and ψ-Values of Glu-29, Tyr-30, Arg-31, and Lys-32 in Individual Helices Averaged over 800 ps in Steps of 1 ps[a]

	bundle 4				bundle 5				bundle 6			
	one helix		second helix		one helix		second helix		one helix		second helix	
residue	ϕ[b]	ψ	ϕ	ψ	ϕ	ψ	ϕ	ψ	ϕ	ψ	ϕ	ψ
Glu-29	−53.7 (9.5)	−30.6 (10.0)	−81.6 (14.3)	−58.6 (11.2)	−56.4 (8.7)	−50.0 (8.1)	−73.5 (12.3)	−31.1 (13.9)	−62.8 (12.5)	−10.1 (31.8)	−78.2 (22.2)	−39.4 (11.9)
Tyr-30	−60.9 (11.2)	−45.7 (11.7)	−61.5 (10.7)	−31.0 (12.6)	−63.8 (10.9)	−23.1 (16.2)	−30.1 (13.8)	−49.7 (11.6)	−98.8 (21.7)	114.0 (7.9)	−53.4 (10.2)	−37.9 (12.0)
Arg-31	−140.2 (20.5)	94.4 (13.5)	−69.4 (18.2)	−10.5 (27.3)	−80.3 (18.7)	−49.4 (10.5)	−43.0 (13.1)	−34.7 (12.3)	−114.8 (8.3)	100.7 (11.8)	−130.1 (12.2)	76.5 (22.0)
Lys-32	−47.7 (15.9)	−73.8 (18.0)	−66.7 (20.4)	−44.2 (15.1)	−62.4 (11.9)	−42.4 (13.4)	−53.6 (13.4)	−24.2 (14.2)	−110.6 (15.2)	−68.5 (11.5)	−109.6 (19.7)	−53.2 (16.9)

[a] The values for the residues within a helix are shown if at least one value deviates more than half of the value for an ideal helix [$\phi = -60°$, $\psi = -50°$ (*35*)]. [b] Values are shown in degrees. Standard deviation is shown in parentheses.

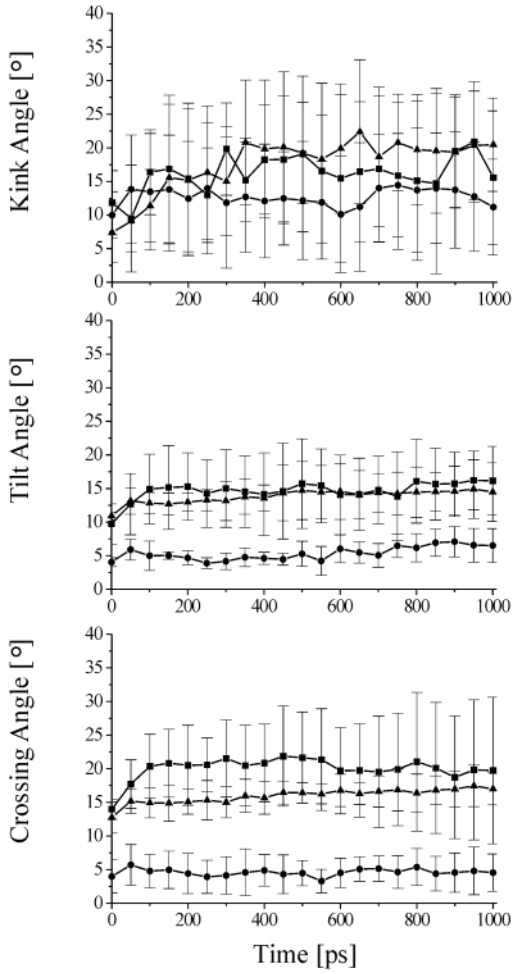

FIGURE 3: Average kink (top), tilt (middle), and crossing angles (bottom) calculated over the number of segments in the bundles [4 (■), 5 (▲), and 6 (●)] for each time frame. Standard deviation is shown (thin lines).

trend of the curves is that they level off after ca. 100 ps. The helices tend to straighten with increasing the bundle size (from 4 to 6). This is supported by a decrease in the average tilt angle for bundle 4 [(15.3 ± 5.0)°] to bundle 6 [(6.0 ± 2.1)°] accompanied by a decrease in the average crossing angle. The average kink angle slightly decreases from (16.9 ± 10.0)° [with one kink angle of (32.1 ± 1.9)°] for bundle 4 to (12.7 ± 7.7)° in bundle 6.

We do not find a continuous water column within bundle 4 at all during the simulation (data not shown). Only three water molecules are found in the immediate vicinity of the

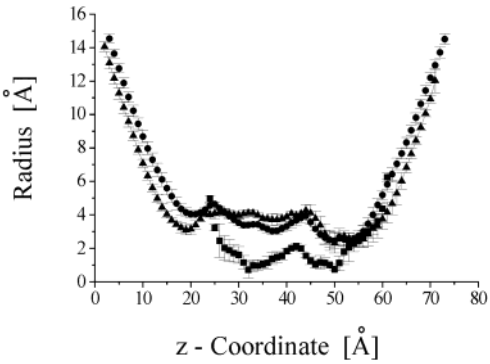

FIGURE 4: Average pore radius across the peptide. Standard deviation is shown from the average of the last five frames covering the last 250 ps of the simulation in steps of 50 ps [(■) bundle 4, (▲) bundle 5, and (●) bundle 6].

Ser-24 residues, forming a hydrophilic, aqueous cage. The average pore radius has a minimum of 0.7 Å (Table 1) around Val-5 and Ser-19 (Figure 4). According to these findings, bundle 4 should not contribute to ion conductance of Vpu on the basis of the simulation studies. However, assessing the conductance based solely on the pore size using the program HOLE (*36*) reveals small values listed in Table 1. The average pore radii for bundle 5 and bundle 6 are around 4 Å with minima caused by Ile-1/Val-2, Ile-11, and Ser-19/Ile-22 facing the pore (Figure 4), resulting in the conductance listed in Table 1. The reason for the low conductance value for bundle 6 might be due to the narrowing of the bundle toward the N-terminal end during the simulation. This narrowing is not completely compensated by the widening on the C-terminal side and accommodated by the program.

To demonstrate channel activity of the TM domain, we used a synthetic peptide analogous to the TM domain of Vpu and almost the same as the domain used for the simulations. Reconstitution of the peptide into model bilayers leads to channel activity as shown in Figure 5. At −100 mV we observe a stepwise increase of conductance to (22 ± 16 SD) pS, (62 ± 28 SD) pS, and (107 ± 17 SD) pS (SD = standard deviation), indicative for the formation of conducting bundles with an increasing number of assembling peptides. Summarizing equivalent stages at different membrane potentials results in levels of [20.7 ± 2.3 (3)] pS, [59.3 ± 4.2 (5)] pS, and [137.0 ± 5.4 (5)] pS (Table 1 and lines in Figure 5A). Occasionally, levels around 30 pS (at +40 and −40 mV) are found as well. We rarely find any clear-cut rectangular-shaped current jumps. Also, once the assembled peptide is in a particular conductance state, we observe relatively noisy

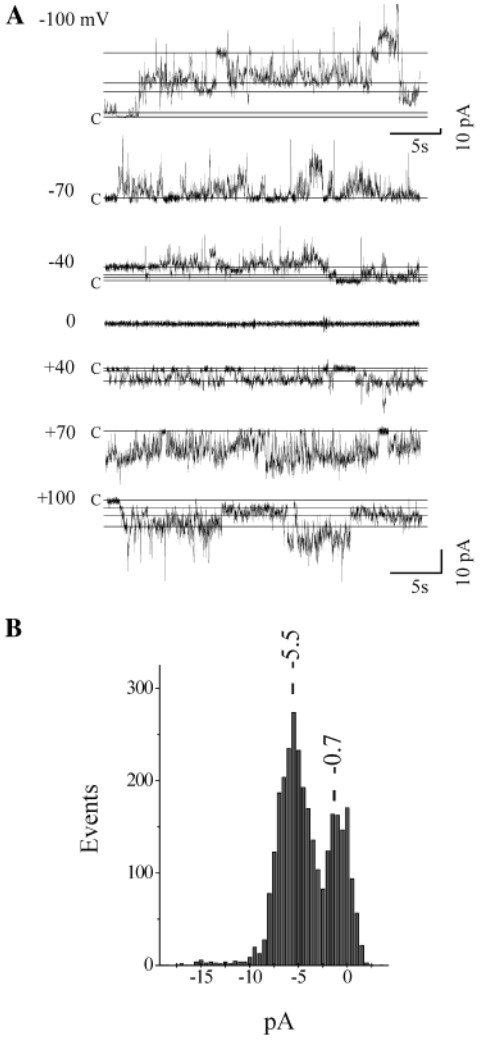

FIGURE 5: (A) Channel activity of the Vpu peptide reconstituted into planar lipid bilayers. Peptide was added to the trans side to reach a final concentration of 30 μM. (B) Representative current histogram for the trace recorded at +40 mV.

recordings which result in a less resolved histogram. Figure 5B shows the histogram for the trace at +40 mV membrane potential. The most important observation is that the conductance at ca. 60 pS corresponds perfectly well with data from computational conductance assessment of bundles with 5 and 6 segments. However, levels below ca. 60 pS are also found in the experiments.

We applied a triangular voltage ramp (±200 mV/10 s) to monitor voltage-dependent channel formation of the TM segments of Vpu (Figure 6). At up to ca. ±90 mV applied membrane potential, we observe linearity in the *I*/*V* curve. Above that potential nonlinearity is found with a slight preference for channel formation at negative cis potential. Having added the peptide on one side of the set up (trans), these results indicate that channels are formed predominately from parallel-orientated helical segments (*37*). Nonlinearity of the current/voltage curve above ca. ±90 mV is indicative for a voltage-dependent channel formation.

DISCUSSION

Reliability of the Generated Models. We have chosen to follow the concept of hydrophilic residues lining the water-filled pore in an ion or proton conducting channel for this

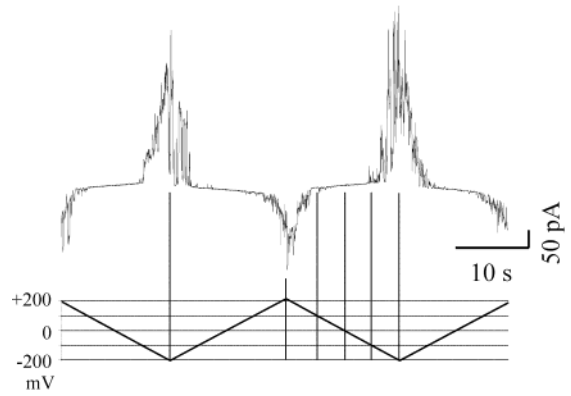

FIGURE 6: Current−voltage diagram for a transbilayer potential of ±200 mV. Representative current responses are shown in the upper trace if a triangular potential (lower trace) is applied.

study. The models presented should consequently account for an "open state" of the channel. The conception of hydrophilic residues lining the pore is based on experimental findings in the pore-lining helices of the nicotinic acetylcholine receptor (nAChR) (*38*−*41*). Computational studies have used these findings to generate not only equivalent bundles of M2 from nAChR (*31*, *32*) but also bundles of the TM domain of the influenza A channel protein M2 (*33*) and the channel protein NB from influenza B (*34*). However, recent studies also show that the positioning of tryptophans toward the center of the pore can result in a model representing a stable "closed" structure (*21*, *24*, *42*).

The simulated bundle 4 does not have any water molecules along the hydrophobic part of the pore. The software GROMACS1.6 does not place any water molecules within the pore because of steric hindrance. The minimum radius (0.7 Å) found at two places within the pore would barely allow for a single water molecule to be placed in this region. The small standard deviation of the values indicates that this narrow region might be stable at least over the time span covered with our simulations. The program HOLE calculates the conductance values on the basis of available space within the pore and therefore yields the plausible values shown in Table 1.

From Structural and Functional Data to the Number of Segments Forming a Channel. We have found in this study a trend suggesting that more segments in a bundle lead to a straightening of the helices. This finding is based on the result of decreasing average kink, tilt, and crossing angles along with increasing bundle size [this behavior has also been observed for NB from influenza B (*34*)]. Vpu exhibits higher average tilt and kink angles for bundle 4 and 5 compared to similar bundles of NB, which have been generated without an initial tilt angle. The average tilt angle for bundle 6 is comparable with that for bundle 6 of NB (ca. 6°). For more helices in a bundle straightening is independent of the initial tilt angle of either 0° or 5°. In a simulation study on bundles corresponding to the tetrameric assembly of the TM helices of the influenza A M2 proton-conducting channel, average tilt angles after 2 ns of simulation seem to be also independent of the initial tilt angle (at 0 ns) but dependent on the length of the segment (*43*). Longer helices tend to remain in a fairly tilted orientation, whereas shorter helices seem to become more upright during the simulation for the particular thickness of the bilayer (POPC) used. For both

the pentameric Vpu bundles of shorter TM helices (22 residues) generated with a starting tilt angle of 5° (*24*) and bundle 5 in this study, we find final tilt angles of around 14−15°. The tilt angles for the TM segments of Vpu are in accord with the experimental findings (*19*, *20*) and seem to be an intrinsic property of the TM helices in smaller Vpu bundles (less than six segments) independent of the length of the TM helices.

With these results about the tilt angle, it is proposed that a considerable kink angle of the TM helices forms in a Vpu bundle, as mentioned above. A pronounced kink is found experimentally for the pore lining helices M2 of the nicotinic acetylcholine receptor (*44*). Computational and experimental data suggest a pentameric bundle to be the main assembly of Vpu. However, hexameric bundles may not be completely ruled out since FTIR data report a very low tilt angle (*21*) which corresponds to the value from computationally derived bundle 6 (Table 1). The overall larger tilt angle for the smaller Vpu bundles compared to the NB bundles could be explained by the large hydrophilic part toward the C-terminal end in the TM helices of Vpu. Helices in tetrameric bundles of M2 from influenza A show large tilt angles [ca. 35° (*45*−*47*)]. It also has one serine and one histidine within the TM segment but is held together by disulfide bonds. Thus, the more extended the hydrophobic pore lining part of a helix within bundle is, the more the helices within bundles of less than six helices tend to tilt by sliding around each other (*48*).

Equally spaced conductance levels reflect the simultaneous opening of two or more channels with similar numbers of segments (*49*). Nonequally spaced current should reflect the increase in conductance due to the association of additional TM peptides. Assuming a cylindrical pore and neglecting the shape of the pore and any electrostatic interactions between ions and the pore, model calculations show that increasing the number of TM peptides decreases the difference between the individual calculated conductance levels. Nonequally spaced conductance levels have been observed for alamethicin (see ref *49* and references cited therein) and also for NB (*34*). The appearance of the nonequally spaced conductance levels for Vpu indicates that the Vpu peptide channels form by stepwise assembly of single TM peptide strands. Once a stable assembly (bundle) is formed (see trace at +40 mV in Figure 5A), a flickering between conductance levels may be caused by fast dynamical structural changes within the assembly. Taking the computational data into account, these dynamics might be caused by residues at the C-terminal end of the peptide. We attribute the higher conductance values to a relatively high peptide concentration in the bilayer which might not reflect the concentration of Vpu found in vivo. It has been shown that Vpu is expressed in equivalent concentrations to the viral membrane proteins gp160 and gp120 (*3*).

The computationally derived conductance data generated here are comparable with the experimentally derived data and those found in the literature for channels formed by full-length Vpu (*11*) and a synthetic TM construct of Vpu (*6*). Even the computationally derived value for bundle 4 has an experimental equivalent for both Vpu types (full-length and TM construct). From the simulations, we have to rule out a tetrameric bundle as an additional functional form besides the favored pentameric bundle (*22*). Relatively long lasting levels around 137 pS could be due to a stable formation of bundles with even more than six TM peptide strands. The derivation of the number of peptide strands forming a bundle by comparison of the computational conductance data with the experimentally derived data has to be treated with caution, since electrostatic interactions of the ions with the pore are ignored (*49*). Our data are in support of an assembly of five or more helices to form a channel.

A Selectivity Filter in Vpu? Experimental findings suggest that Vpu has a weak preference of cations over anions (*11*). In a recent computational approach, ion selectivity is attributed to the ring of serines-24 pointing into the pore (*22*). With their oxygen atoms, serines are well suited to be responsible for the experimentally found selectivity. However, cation preference has been found to be weak. In our models, arginines (Arg-31) are pointing into the pore forming a positively charged ring (Figure 2B). The ring of positively charged arginines could lower the barrier for anions to pass the pore. Alamethicin mutants in which a glutamine (Gln-18) is replaced by lysine have been shown to change the slight cation selectivity into a preference for anions for this channel (*50*, *51*). Arginine with its flexible side chain would be also a plausible candidate for temporarily blocking the pore.

Is Vpu Forming an Ion Channel? There is debate about whether full-length Vpu fulfills a biological role by forming an ion channel (*14*). Even though our results might not contribute directly to this discussion, we do show channel activity of the synthetic TM peptide analogous to the Vpu TM domain, reconstituted in a lipid bilayer. Recent discovery of drugs decreasing the number of released virus particles and blocking channel activity of reconstituted full-length Vpu and peptides analogous to the TM domain can be seen as providing a missing piece of the puzzle in the debate on the in vivo ion channel activity of Vpu (*15*).

CONCLUSIONS

From our results we draw the following conclusions: (i) the average tilt angle decreases slightly with an increasing number of helices in the bundle from 4 to 6; (ii) it seems to be an intrinsic property of pore-lining helices to adopt a kinked structure within the bilayer; (iii) one of the roles of the EYR motif might be to form a positively charged selectivity filter.

We cannot rule out the existence of bundles with more than five TM peptides contributing to the functional state of the Vpu peptide under investigation. It is up to further experimental studies to establish more accurately the number of TM peptides/full-length proteins involved in forming functional Vpu ion channels.

ACKNOWLEDGMENT

We acknowledge the gift of the Vpu peptide from P. Gage.

REFERENCES

1. Strebel, K., Klimkait, T., and Martin, M. A. (1988) *Science 241*, 1221−1223.
2. Cohen, E. A., Terwilliger, E. F., Sodroski, J. G., and Haseltine, W. A. (1988) *Nature 334*, 532−534.
3. Strebel, K., Klimkait, T., Maldarelli, F., and Martin, M. A. (1989) *J. Virol. 63*, 3784−3791.
4. Willey, R. L., Maldarelli, F., Martin, M. A., and Strebel, K. (1992) *J. Virol. 66*, 7193−7200.

5. Bour, S., Schubert, U., and Strebel, K. (1995) *J. Virol. 69*, 1510−1520.
6. Schubert, U., Ferrer-Montiel, A. V., Oblatt-Montal, M., Henklein, P., Strebel, K., and Montal, M. (1996) *FEBS Lett. 398*, 12−18.
7. Schubert, U., Bour, S., Ferrer-Montiel, A. V., Montal, M., Maldarelli, F., and Strebel, K. (1996) *J. Virol. 70*, 809−819.
8. Paul, M., Mazumder, S., Raja, N., and Jabbar, M. A. (1998) *J. Virol. 72*, 1270−1279.
9. Deora, A., Spearman, P., and Ratner, L. (2000) *Virology 269*, 305−312.
10. Kerkau, T., Bacik, I., Bennink, J. R., Yewdell, J. W., Hunig, T., Schimpl, A., and Schubert, U. (1997) *J. Exp. Med. 185*, 1295−1305.
11. Ewart, G. D., Sutherland, T., Gage, P. W., and Cox, G. B. (1996) *J. Virol. 70*, 7108−7115.
12. Maldarelli, F., Chen, M. Y., Willey, R. L., and Strebel, K. (1993) *J. Virol. 67*, 5056−5061.
13. Coady, M. J., Daniel, N. G., Tiganos, E., Allain, B., Friborg, J., Lapointe, J.-Y., and Cohen, E. A. (1998) *Virology 244*, 39−49.
14. Lamb, R. A., and Pinto, L. H. (1997) *Virology 229*, 1−11.
15. Ewart, G. D., Mills, K., Cox, G. B., and Gage, P. W. (2001) *Eur. Biophys. J.* (in press).
16. Wray, V., Federau, T., Henklein, P., Klabunde, S., Kunert, O., Schomburg, D., and Schubert, U. (1995) *Int. J. Pept. Protein Res. 45*, 35−43.
17. Federau, T., Schubert, U., Flossdorf, J., Henklein, P., Schomburg, D., and Wray, V. (1996) *Int. J. Pept. Protein Res. 47*, 297−310.
18. Willbold, D., Hoffmann, S., and Rösch, P. (1997) *Eur. J. Biochem. 245*, 581−588.
19. Wray, V., Kinder, R., Federau, T., Henklein, P., Bechinger, B., and Schubert, U. (1999) *Biochemistry 38*, 5272−5282.
20. Marassi, F. M., Ma, C., Gratkowski, H., Straus, S. K., Strebel, K., Oblatt-Montal, M., Montal, M., and Opella, S. J. (1999) *Proc. Natl. Acad. Sci. U.S.A. 96*, 14336−14341.
21. Kukol, A., and Arkin, I. T. (1999) *Biophys. J. 77*, 1594−1601.
22. Grice, A. L., Kerr, I. D., and Sansom, M. S. P. (1997) *FEBS Lett. 405*, 299−304.
23. Moore, P. B., Zhong, Q., Husslein, T., and Klein, M. L. (1998) *FEBS Lett. 431*, 143−148.
24. Cordes, F., Kukol, A., Forrest, L. R., Arkin, I. T., Sansom, M. S. P., and Fischer, W. B. (2001) *Biochim. Biophys. Acta 1512*, 291−298.
25. Zheng, S., Strzalka, J., Ma, C., Opella, S. J., Ocko, B. M., and Blasie, J. K. (2001) *Biophys. J. 80*, 1837−1850.
26. Kerr, I. D., Sankararamakrishnan, R., Smart, O. S., and Sansom, M. S. P. (1994) *Biophys. J. 67*, 1501−1515.
27. Brünger, A. T. (1992) *X-PLOR Version 3.1. A System for X-ray Crystallography and NMR*, Yale University Press, New Haven, CT.
28. Berendsen, H. J. C., Grigera, J. R., and Straatsma, T. P. (1987) *J. Phys. Chem. 91*, 6269−6271.
29. Fischer, W. B., Forrest, L. R., Smith, G. R., and Sansom, M. S. P. (2000) *Biopolymers 53*, 529−538.
30. Montal, M., and Mueller, P. (1972) *Proc. Natl. Acad. Sci. U.S.A. 69*, 3561−3566.
31. Sankararamakrishnan, R., Adcock, C., and Sansom, M. S. P. (1996) *Biophys. J. 71*, 1659−1671.
32. Ortells, M. O., Barrantes, G. E., Wood, C., Lunt, G. G., and Barrantes, F. J. (1997) *Protein Eng. 10*, 511−517.
33. Forrest, L. R., Tieleman, D. P., and Sansom, M. S. P. (1999) *Biophys. J. 76*, 1886−1896.
34. Fischer, W. B., Pitkeathly, M., Wallace, B. A., Forrest, L. R., Smith, G. R., and Sansom, M. S. P. (2000) *Biochemistry 39*, 12708−12716.
35. Branden, C., and Tooze, J. (1991) *Introduction to Protein Structure*, Garland, New York.
36. Smart, O. S., Breed, J., Smith, G. R., and Sansom, M. S. P. (1997) *Biophys. J. 72*, 1109−1126.
37. Kerr, I. D., Dufourcq, J., Rice, J. A., Fredkin, D. R., and Sansom, M. S. P. (1995) *Biochim. Biophys. Acta 1236*, 219−227.
38. Leonard, R. J., Labarca, C. G., Charnet, P., Davidson, N., and Lester, H. A. (1988) *Science 242*, 1578−1581.
39. Charnet, P., Labarca, C., Leonard, R. J., Vogelaar, N. J., Czyzyk, L., Gouin, A., Davidson, N., and Lester, H. A. (1990) *Neuron 2*, 87−95.
40. Villarroel, A., Herlitze, S., Koenen, M., and Sakmann, B. (1991) *Proc. R. Soc. London, Ser. B 243*, 69−74.
41. Imoto, K., Konno, T., Nakai, J., Wang, F., Mishina, M., and Numa, S. (1991) *FEBS Lett. 289*, 193−200.
42. Sansom, M. S. P., Kerr, I. D., Smith, G. R., and Son, H. S. (1997) *Virology 233*, 163−173.
43. Forrest, L. R., Kukol, A., Arkin, I. T., Tieleman, D. P., and Sansom, M. S. P. (2000) *Biophys. J. 78*, 55−69.
44. Unwin, N. (1993) *J. Mol. Biol. 229*, 1101−1124.
45. Kovacs, F. A., and Cross, T. A. (1997) *Biophys. J. 73*, 2511−2517.
46. Kovacs, F. A., Denny, J. K., Song, Z., Quine, J. R., and Cross, T. A. (2000) *J. Mol. Biol. 295*, 117−125.
47. Kukol, A., Adams, P. D., Rice, L. M., T., B. A., and Arkin, I. T. (1999) *J. Mol. Biol. 286*, 951−962.
48. Kerr, I. D., Sankararamakrishnan, R., Smart, O. S., and Sansom, M. S. P. (1994) *Biophys. J. 67*, 1501−1515.
49. Sansom, M. S. P. (1991) *Prog. Biophys. Mol. Biol. 55*, 139−236.
50. Starostin, A. V., Butan, R., Borisenko, V., James, D. A., Wenschuh, H., Sansom, M. S. P., and Woolley, G. A. (1999) *Biochemistry 38*, 6144−6150.
51. Borisenko, V., Sansom, M. S. P., and Woolley, G. A. (2000) *Biophys. J. 78*, 1335−1348.

BI025518P